Journal of Molecular Graphics and Modelling 33 (2012) 1–11

Contents lists available at SciVerse ScienceDirect

Journal of Molecular Graphics and Modelling

journal homepage: www.elsevier.com/locate/JMGM

Specific interactions and binding energies between thermolysin and potent inhibitors: Molecular simulations based on *ab initio* molecular orbital method

Tatsuya Hirakawa [a], Seiya Fujita [a], Tatsuya Ohyama [a], Kenichi Dedachi [a], Mahmud Tareq Hassan Khan [b,1], Ingebrigt Sylte [b], Noriyuki Kurita [a,*]

[a] *Department of Computer Science and Engineering, Toyohashi University of Technology, Tempaku-cho, Aichi 441-8580, Japan*
[b] *Medical Pharmacology and Toxicology, Department of Medical Biology, Faculty of Health Sciences, University of Tromsø, 9037 Tromsø, Norway*

ARTICLE INFO

Article history:
Received 11 August 2011
Received in revised form 18 October 2011
Accepted 18 October 2011
Available online 2 November 2011

Keywords:
Thermolysin
Inhibitor
Specific interaction
Molecular simulations
Classical molecular mechanics
Ab initio molecular orbital

ABSTRACT

Biochemical functions of the metalloprotease thermolysin (TLN) are controlled by various inhibitors. In a recent study we identified 12 compounds as TLN inhibitors by virtual screening and *in vitro* competitive binding assays. However, the specific interactions between TLN and these inhibitors have not been clarified. We here investigate stable structures of the solvated TLN–inhibitor complexes by classical molecular mechanics simulations and elucidate the specific interactions between TLN and these inhibitors at an electronic level by using *ab initio* fragment molecular orbital (FMO) calculations. The calculated binding energies between TLN and the inhibitors are qualitatively consistent with the experimental results, and the FMO results elucidate important amino acid residues of TLN for inhibitor binding. Based on the calculated results, we propose a novel potent inhibitor having a large binding affinity to TLN.

1. Introduction

Thermolysin (TLN) is a Zn metalloprotease secreted by the gram-positive thermophilic bacterium *Bacillus thermoproteolyticus*. TLN has high thermal stability [1] assisted by four structural Ca ions, and catalyses the hydrolysis of peptide bonds containing hydrophobic amino acid residues [2]. One catalytic Zn ion is required for the hydrolysis function of TLN [3]. In addition to these ions, the binding of a wide variety of inhibitors controls efficiently the chemical activity and biochemical functions of TLN. Previous experiments [2,4,5] elucidated that amino acids of the four sub-pockets in the substrate binding region of TLN (S1, S1', S2 and S2') provide a significant contribution to the specificity of ligand binding.

TLN has been widely used by the chemical industry, including for the synthesis of a precursor of the artificial sweetener aspartame ZDFM [6–10]. Reducing synthetic costs by enhancing the enzymatic activity of TLN is therefore of considerable industrial value. For this purpose, its catalytic mechanisms and recombinants have been widely studied both by experimental [11–16] and theoretical [17–22] studies. However, the mechanism has not yet been clarified at atomic and electronic levels.

TLN, which is the prototype of the M4 family of proteinases, and other bacterial enzymes of the M4 family are believed to be important for suppressing or avoiding the innate immune system of the infected host during pathogenesis [23]. The inhibition of the activity of TLN and these enzymes is expected to be a novel strategy in developing the new generation of antibacterial drugs [24,25]. Zn metalloproteinases with close structural and functional similarities to TLN are named thermolysin-like proteinases (TLPs). They contain the consensus amino acid sequence HExxH forming a part of the Zn-containing catalytic domain [10]. Several TLPs play important roles for controlling different physiological functions. For example, the TLP angiotensin-converting enzyme (ACE) is involved in the control of hypertension, and ACE inhibitors have a therapeutically potential in the treatment of hypertension, heart failure and diabetic nephropathy [26]. For developing potent inhibitors of TLPs with therapeutically potentials, it is indispensable to elucidate the specific interactions between the enzymes and various ligand molecules. The determination of 3-dimensional (3D) structures of TLPs and their complexes with ligand is still not straight forward, and molecular modeling may be an alternative for gaining structural insight. Due to structural similarities among TLPs, crystallographic data of TLN and various TLN–inhibitor complexes have also been used to construct model structures of other TLPs. In addition, the functional similarity between TLN and TLPs

* Corresponding author. Tel.: +81 532 44 6875; fax: +81 532 44 6875.
E-mail address: kurita@cs.tut.ac.jp (N. Kurita).
[1] Present address: Center for Pharmaceutical Biotechnology, College of Pharmacy, University of Illinois at Chicago, Chicago, IL 60607-7173, USA.

1093-3263/$ – see front matter © 2011 Elsevier Inc. All rights reserved.
doi:10.1016/j.jmgm.2011.10.006

indicates that TLN inhibitors also may inhibit the activity of other TLPs. Therefore, various TLN inhibitors are developed and experimentally tested [27,28].

By structure-based virtual ligand screening (VLS) techniques, we have previously identified 22 molecules as putative TLN inhibitors, and 12 of them were confirmed as TLN binders by *in vitro* competitive binding assays [29]. Furthermore, by use of the molecular modeling program ICM (Internal Coordinate Mechanics) [30–32], the binding modes and affinities of these inhibitors to TLN were predicted, giving a good correlation ($R^2 = 0.78$) between the ICM scoring value and the experimental detected IC_{50} values [29]. These predictions and our more recent studies [33,34] indicated that the binding modes and affinities are largely dependent on the type of inhibitor, although their chemical structures are quite similar to each other. The origin for this large dependency of binding affinity has not been clarified at the electronic level. In the present study, we further investigate the binding of five of the inhibitors from the VLS study to TLN by studying stable structures of solvated TLN–inhibitor complexes by classical molecular mechanics (MM) simulations. The specific interactions between TLN and the inhibitors are elucidated by *ab initio* fragment molecular orbital (FMO) calculations with solvating water molecules considered explicitly. The calculated binding energies are qualitatively consistent with the observed trend of the experimental inhibition [29]. We furthermore elucidate which amino acid residues in TLN are important for the specific binding between TLN and inhibitors at an electronic level.

2. Methods of calculations

2.1. Classical MM optimizations for solvated TLN–ligand complexes

TLN–ligand complexes from our previous study [29] were used as initial structures for the calculations. These complexes were obtained by the ICM-Docking program [30–32]. The structures of the five ligands (Nx, x = 1–5) employed here are shown in Fig. 1. Hydrogen atoms were added to the complexes, and the positions of the hydrogen atoms were optimized by the classical MM program package AMBER9 [35]. In order to obtain a solvated structure of TLN–ligand complex, solvating water molecules (about 4500) were added within 8 Å from the surface of the complex. The positions of only the solvating water molecules were optimized to reduce steric clashes between the water molecules and the complex. Since the ligand N3 is so small giving a wide space around N3 in the ligand-binding pocket of the solvated TLN–N3 complex, the structure of the solvated TLN–N3 complex was fully optimized by AMBER9 to obtain more stable conformation of N3. The PARM99 [36] and TIP3P [37] force fields were used for the complex and the water molecules, respectively. The charges for each atom of the ligands were determined from the restrained electrostatic potential (RESP) analysis [38] based on the MP2/6-31G(d,p) method [39] of the *ab initio* MO program Gaussian03 [40]. The force field parameters for Zn and Ca ions in TLN were constructed by using the antechamber program of AMBER9 [35]. The charges of these ions were set to 2.0.

2.2. FMO calculations for solvated TLN–ligand complexes

In order to elucidate the specific interactions between TLN and ligands at an electronic level, electronic properties of the solvated TLN–ligand complexes were investigated by the multilayer FMO (MFMO) method [41–46] implemented in the ABINIT-MP ver.4.1 program [47]. MFMO calculations of fully solvated TLN–ligand complexes are not practical to perform, since these complexes contain around 4500 solvating water molecules. Water molecules existing far away from the ligand and the Zn ion do not have a large influence on the TLN–ligand interactions, and therefore only water molecules existing within 5 Å from the ligand or Zn ion were considered in the MFMO calculations. In FMO calculations, the target molecule is divided into units called fragments, and the electronic properties of the target molecule are estimated from the electronic properties of the monomers and dimers of the fragments. Since the electronic properties of the dimers are calculated in FMO, we can obtain the interaction energies between specific fragments with the effect from the other fragments considered. This pair interaction energy, also called inter-fragment interaction energy (IFIE) [48–50], is somewhat similar to the simple pair interaction energy computed by classical force field methods. However, in the FMO evaluation of the pair interaction energy, the influence from other fragments is taken into account as a direct coulomb interaction. In addition, the charge redistribution around the binding site induced by ligand binding is considered in FMO calculations, whereas classical MM method uses a fixed charge parameter for ligand-free and ligand-bound proteins. In the present study, the fragment size was set as one amino acid residue or one water molecule. We thus investigated the interaction energies between the ligand and each amino acid residue of TLN or each solvating water molecule, in order to elucidate which residues in TLN are important for ligand binding. The effect of solvating water molecules on specific ligand interactions was also elucidated. To describe electronic states around the Zn ion more precisely, the Zn ion was included in the same fragment as His142, His146 and Glu166 existing near the Zn ion, as explained in our previous studies [51,52].

In the present MFMO calculations, the electronic properties around the ligand were evaluated accurately by MP2/6-31G method which considers electron correlation effects, while the effect of the amino acid residues existing far from the ligand was treated by HF/6-31G method, because the electron correlation effects of these residues are negligible. In fact, the ligand, the amino acid residues of TLN and water molecules existing within 5 Å from the ligand were treated by MP2/6-31G, while the other residues and water molecules were treated by HF/6-31G.

In order to investigate the binding energy between TLN and the ligand, the solvated TLN–ligand structure was divided into the following three structural domains: TLN–ligand complex containing solvating water molecules (TLN + ligand + water), TLN containing solvating water molecules (TLN + water) and ligand. The structures of TLN + water and ligand were extracted from the optimized structure of TLN + ligand + water. From their total energies (T.E.) obtained by the MFMO calculations, the binding energy (B.E.) between TLN and the ligand mediated by solvating water molecules was estimated as B.E. = T.E. (TLN + ligand + water) − T.E. (TLN + water) − T.E. (ligand). It is noted that the basis set superposition error was neglected in the analysis of binding energy between TLN and the ligands.

In order to elucidate binding affinity between TLN and the ligands quantitatively, binding free energy should be evaluated. However, it is not practical to calculate free energies for the solvated TLN–ligand complexes by *ab initio* FMO method. In the present study, we thus investigated the binding energies between TLN and the ligands to estimate the binding affinity between them qualitatively, on the assumption that the entropic effects for the solvated TLN–ligand complexes are almost similar.

3. Results and discussion

3.1. Optimized structures of solvated TLN–ligand complexes

Of the 12 compounds confirmed as TLN inhibitors in our previous study [29], five were selected and investigated for their specific TLN interactions in the present study. The structures of the five

Table 1
Total energies (kcal/mol) of solvated TLN–Nx, TLN, Nx, and estimated binding energies (B.E.) (kcal/mol) between TLN and Nx, and the experimentally obtained K_i values (mM) and IC_{50} values (mM) [29] for TLN–Nx complexes. For the small N3 ligand, the results for the complexes of TLN with both one and two N3 binding are listed, while for the N2 ligand with a chain part, the result for the modified ligand without the chain part is listed.

	Total energy			B.E.	K_i	IC_{50}
	TLN–Nx–water	TLN–water	Nx			
Nl	−79910785.2	−78923915.9	−986771.0	−98.3	670	697.48
N2	−79821454.3	−78923876.2	−897461.4	−116.7	6.4×10^{-7}	6.4×10^{-8}
N3	−79222121.0	−78923999.8	−298053.2	−67.9	0.214	0.35
$2 \times$ N3	−79520206.8	−78923983.8	−596116.8	−106.3	0.214	0.35
N4	−79543406.1	−78923928.2	−619366.3	−111.6	2.95	29.5
N5	−79806830.7	−78923895.4	−882823.5	−111.8	0.047	0.047
N2 (no chain)	−79576210.9	−78923954.4	−652121.1	−135.4	–	–

ligands (Nx, x = 1–5) are shown in Fig. 1. The compounds N2, N3 and N5 were selected based on their high TLN binding affinity, while N1 and N4 were selected because they have chemical structures very similar to that of N5 and rather low TLN binding affinity. As listed in Table 1, the experimentally obtained K_i value (inhibition constant) and IC_{50} value (half maximal (50%) inhibitory concentration) for the inhibition of TLN by N1 is about 10^4 times larger than that of N5, indicating that N5 binds about 10^4 times stronger to TLN than do N1. This large difference in binding affinity between N1 and N5 cannot be directly explained by their structural difference shown in Fig. 1, and it is therefore necessary to elucidate their specific interactions with TLN for explaining their binding affinity differences. For this purpose, we first optimized the structures of the solvated TLN–Nx complexes by AMBER9 [35]. The optimized structure of solvated TLN is shown in Fig. 2, where solvating water molecules are not displayed for clarifying the structure of TLN around Nx ligand. Additionally, for the optimized structures of the solvated TLN–Nx complexes, the structures around the Nx ligand are compared in Fig. 3.

As shown in Fig. 1, compounds N1, N4 and N5 have similar backbone structure composed of two hexagonal rings. However, their structures in the binding pocket of TLN seem to be remarkably different, as shown in Fig. 3(a), (d) and (e). In the TLN–N1 and TLN–N4 complexes, the two hexagonal rings are vertically located to each other, whereas the rings of N5 are oriented parallel to each other (Fig. 3e). Therefore, it is elucidated that the strong inhibitor N5 has a nearly planar structure in the ligand-binding pocket of TLN.

The strongest inhibitor N2, which has a dodecyl chain ($-(CH_2)_{11}-CH_3$) as well as pentagonal and hexagonal rings, is stabilized into a non-planar and folded shape in the TLN binding pocket, as shown in Fig. 3(b). The previous experimental study [29] indicated that N3 is a stronger TLN inhibitor than N1 and N4 but weaker than N2 and N5. Fig. 3(c) indicates that N3 is stabilized as a planar structure in the pocket, and that there also is enough space in the

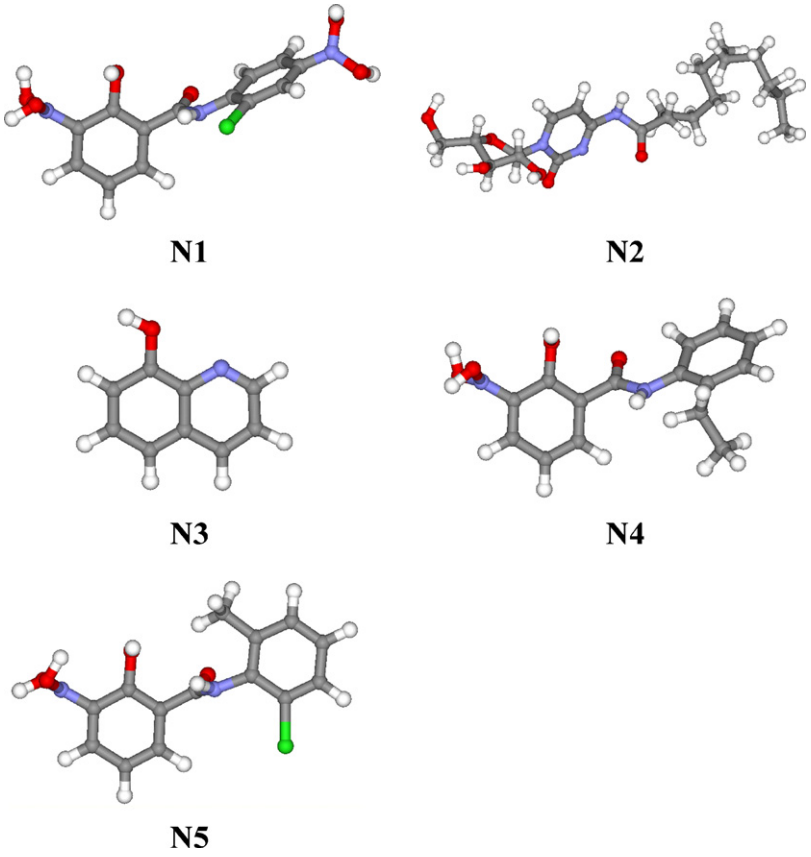

Fig. 1. Structures of five Nx inhibitors to TLN employed in the present study. Chlorine, hydrogen, carbon, oxygen and nitrogen atoms are shown in green, white, gray, red and blue colors, respectively. (For interpretation of the references to color in this figure legend, the reader is referred to the web version of the article.)

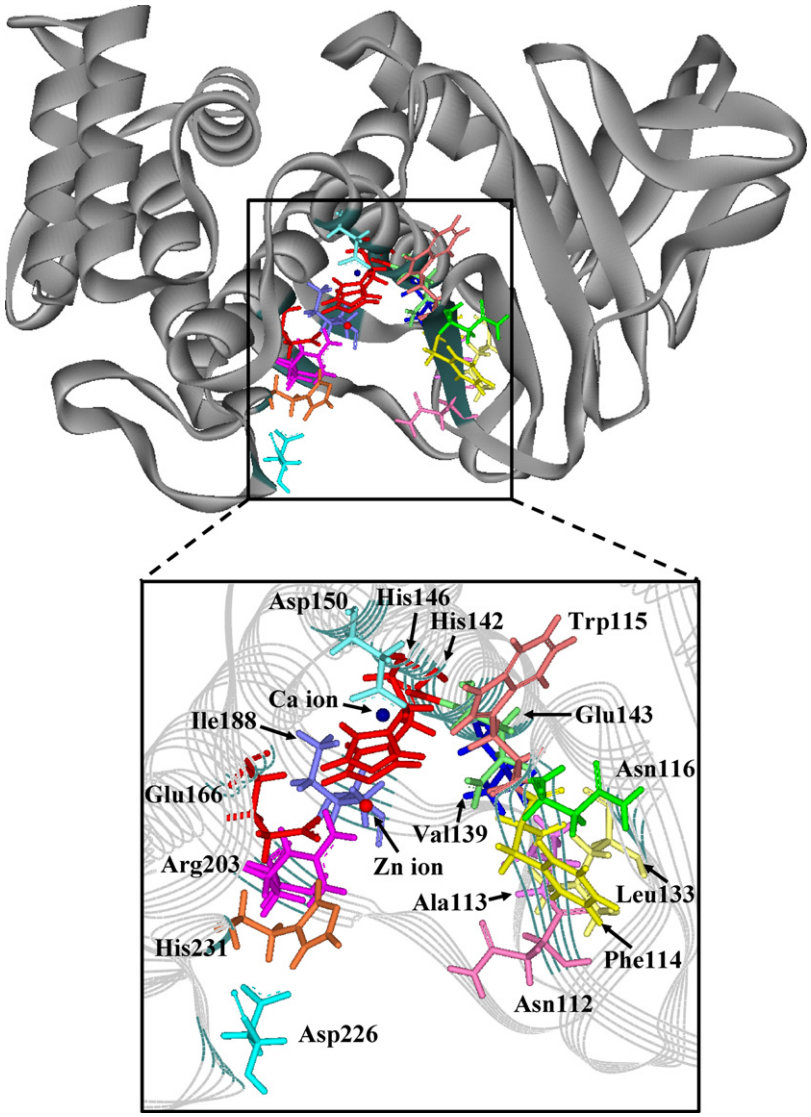

Fig. 2. Optimized structure of solvated TLN. Solvating water molecules are not shown for clarifying the TLN structure. A close-up view around the ligand-binding pocket of TLN and some important amino acid residues for ligand binding is shown in the lower panel.

ligand-binding pocket for binding of an additional N3 molecule. We thus docked an additional N3 molecule into the ligand-binding pocket of TLN–N3 complex by using the automated protein-ligand docking program AutoDock 4.2 [53] and optimized the solvated structure of TLN–2 × N3 by AMBER9 [35]. As shown in Fig. 3(f), the docked N3 binds near the Zn ion and is stacked to the other N3 in the ligand-binding pocket of TLN.

In order to elucidate the difference in specific interactions between TLN and Nx, we analyzed the hydrogen bonding structures around the Nx inhibitors. As indicated in Fig. 4, the numbers of the hydrogen bonds between TLN or water molecules and Nx are 7 (N1), 9 (N2), 1 (N3), 3 (N4), 6 (N5) and 4 (2 × N3), respectively. In the solvated TLN–N2 complex (Fig. 4b), 6 water molecules are hydrogen bonded to the ring system of N2, while there is no water molecule around the hydrophobic chain of N2. In the TLN–N1 and TLN–N5 complexes, one unique water molecule acts as a bridge between N1/N5 and Trp115 of TLN to enhance the binding. On the other hand, there is no water molecule around N3 and N4. Accordingly, it is elucidated that the hydration around the inhibitors Nx in the ligand-binding pocket of TLN is largely dependent on the chemical structure of the inhibitor. This difference in hydration is expected to affect the binding affinity between TLN and Nx.

Fig. 4 also indicates the important amino acid residues of TLN for the TLN–Nx binding. Trp115 is hydrogen bonded to N1, N4 and N5, while Glu143 is bonded to all Nx ligands. In addition, Asp150 is bonded to N2, and Asn112 and Ala113 are bound to N3. These residues in TLN are likely to provide efficient contributions to the binding between TLN and Nx.

3.2. Specific interactions between TLN and ligands

To estimate the binding affinity between TLN and the ligand Nx, the binding energy between TLN and Nx was evaluated with the water molecules in the complex considered explicitly. Table 1 lists the total energies of the component structures of the solvated TLN–ligand complexes, the estimated binding energies between TLN and Nx, and the K_i values and the IC_{50} values obtained by the previous experimental study [29]. The binding energy between TLN and N3 is remarkably smaller than those for the other compounds, in spite of the similar K_i value of N3 to the other ligands. This indicates that the binding energy calculated for TLN–N3 complex cannot explain the trend of the binding affinity between TLN and Nx obtained by the experimental study. Docking of a second N3 molecule into the TLN–N3 complex improved the correlation

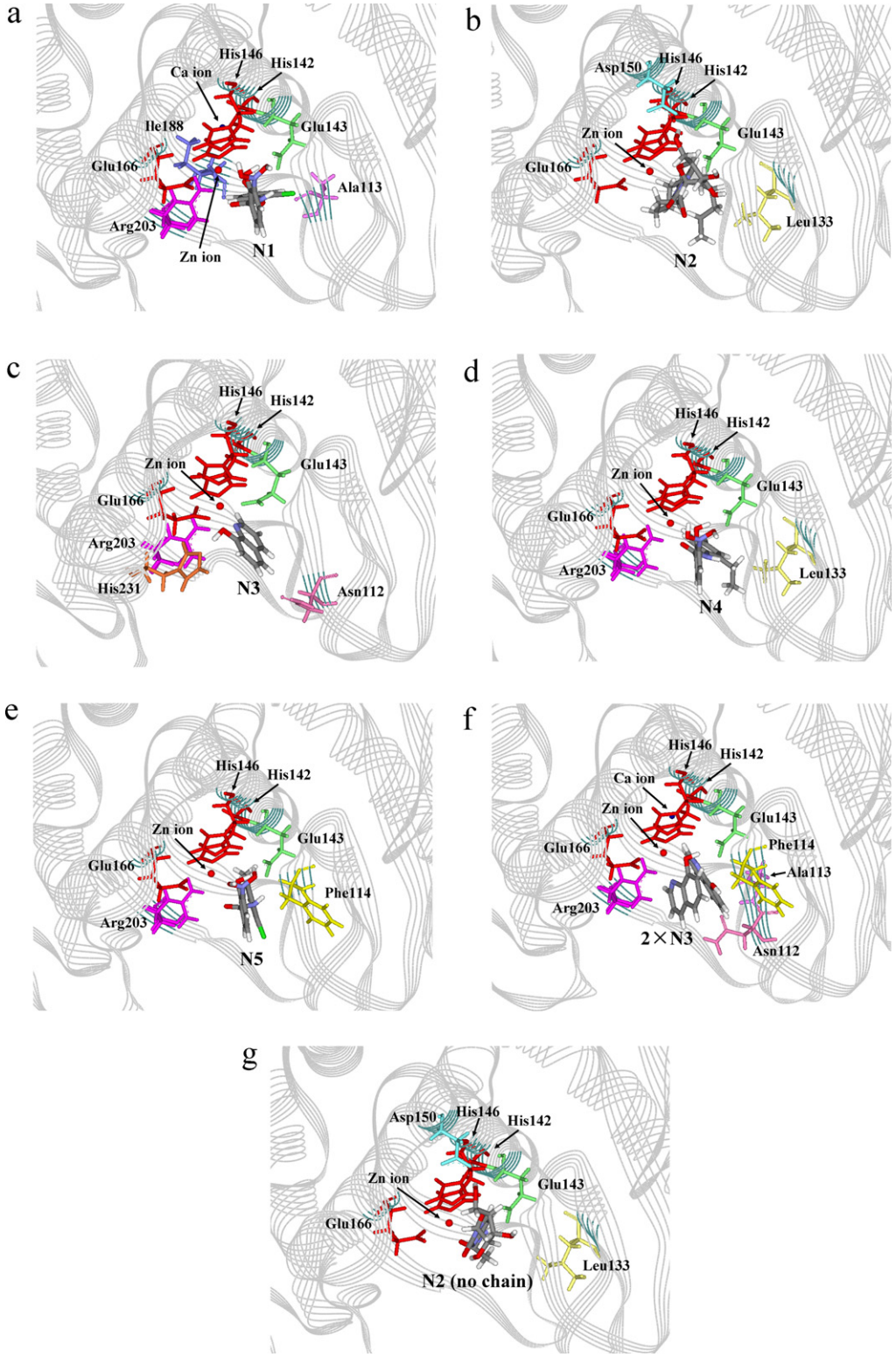

Fig. 3. Close-up views around the ligand-binding pocket of TLN and ligand Nx for the optimized structures of the solvated TLN–Nx complexes: (a) TLN–N1, (b) TLN–N2, (c) TLN–N3, (d) TLN–N4, (e) TLN–N5, (f) TLN–2 × N3, and (g) TLN–N2(no chain). Some amino acid residues of TLN interacting to Nx are indicated.

with the experimental result, and thus we consider the optimized structure of TLN–2 × N3 as the realistic complex of TLN with N3 ligands. The scatter plots of the K_i values and the calculated binding energies for the TLN–Nx complexes are shown in Fig. 5. The correlation coefficient R^2 between the K_i value and these binding energies was found to be 0.72, indicating that there is a reasonable correlation between them. Consequently, we concluded that the calculated binding energies can describe the trend of binding affinity between TLN and the Nx ligands.

In order to elucidate which amino acid residues of TLN that contribute to the binding between TLN and Nx, we investigated the interaction energies between each residue of TLN and Nx ligands using the MFMO calculations. The obtained inter-fragment interaction energies for the TLN–Nx complexes are compared in Fig. 6,

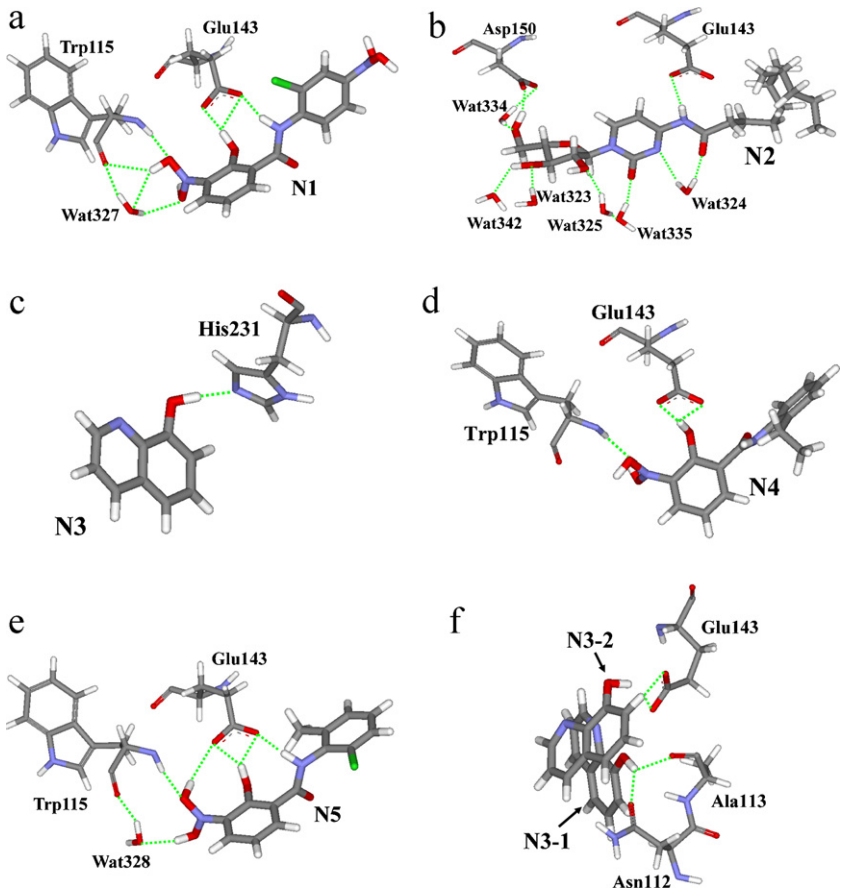

Fig. 4. Hydrogen bonding structures between amino acid residues of TLN or water molecules and (a) N1, (b) N2, (c) N3, (d) N4, (e) N5 and (f) two N3. Chlorine, hydrogen, carbon, oxygen and nitrogen atoms are shown in green, white, gray, red and blue colors, respectively. Hydrogen bonds are indicated by green dot-lines. (For interpretation of the references to color in this figure legend, the reader is referred to the web version of the article.)

where the asterisk indicates the fragment composed of the Zn ion, His142, His146 and Glu166 residues located close to the Zn ion. This fragment, which is defined as the Zn group below, has strong attractive interactions with all Nx ligands. The negatively charged atoms of the ligands are likely to contribute to the interactions. In particular, the interaction energy between N4 and the Zn group is very favorable (−179 kcal/mol), so that the binding affinity between TLN and N4 is mainly determined by the interaction between the catalytic Zn group and N4.

The negatively charged Glu143 of TLN interacts strongly with N1, N3, N4 and N5. In particular, N5 interacts strongly (−62.3 kcal/mol) with Glu143, because N5 has four hydrogen bonds

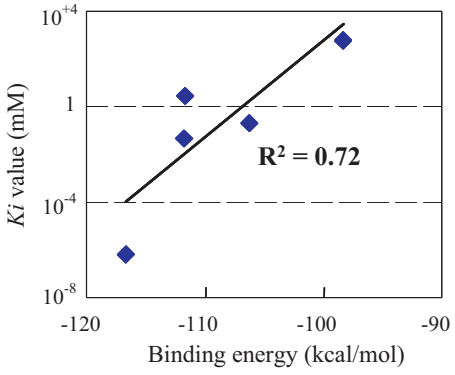

Fig. 5. Scatter plots of the K_i values obtained in the previous experiment [29] and the calculated binding energies for the TLN–Nx complexes. For N3 ligand, the binding energy for the TLN–2 × N3 complex is included.

with Glu143 as shown in Fig. 4(e). In contrast, the interaction energy of Glu143 with N1/N4 is much smaller than that for N5, although the chemical structures of N1 and N4 are quite similar to that of N5. This difference in interaction energies is considered to be a result of the direction of hydroxyl groups of these inhibitors. In the TLN–N5 complex, two hydroxyl groups of N5 are directed to the carboxylate group of Glu143 forming hydrogen bonds, as shown in Fig. 4(e). On the other hand, only one hydroxyl group forms a hydrogen bond with Glu143 in the TLN–N1 (Fig. 4a) and TLN–N4 (Fig. 4d) complexes. Although the chemical structure of the hexagonal ring contributing to the binding between Glu143 and Nx (x = 1, 4 and 5) are similar for these inhibitors, their detailed interactions with Glu143 are different, reflecting differences in chemical structure of the substituted group on the other hexagonal ring.

In addition, Arg203 interacts attractively with N1, N3, N4 and N5, while Leu133 interacts repulsively with N2 and N4. Asp150 interacts attractively with only N2. It is also noted that N2 interacts attractively with many solvating water molecules.

As indicated in Table 1, the binding affinities between TLN and N1, N4 and N5 are remarkably different to each other, although their chemical structures are almost similar. In order to elucidate the origin of these differences, we investigated the difference in interaction energies between each amino acid residue of TLN and these three inhibitors. As shown in Fig. 7, the difference between N5 and N1 is remarkable for Asn112, Ala113, Asn116, Zn group, Glu143, Ile188 and Ca ions, while the difference between N5 and N4 is remarkable for Asn112, Leu133, Zn group and Glu143. As for the difference between N4 and N1, Leu133, Zn group, Glu143, Ile188 and Ca ions have different interaction energies. The Zn group of TLN interacts strongly with N4, while Glu143 interacts with N5. The

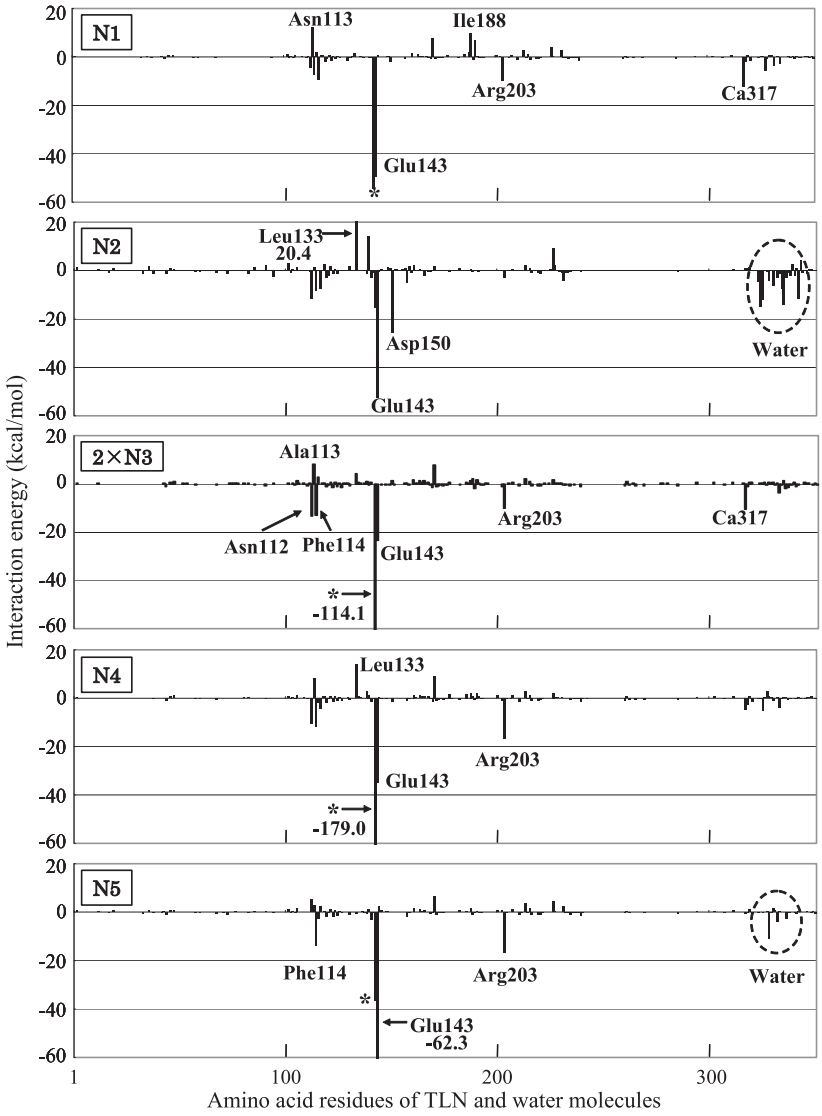

Fig. 6. Interaction energies between amino acid residues of TLN or water molecules and the Nx ligands obtained by MFMO calculations. The asterisk indicates the fragment composed of Zn ion, His142, His146 and Glu166 residues of TLN existing near the Zn ion.

interaction between Leu133 and N4 is strong, while Ile188 interacts strongly with N1, as indicated in Figs. 6 and 7.

To elucidate the reason for the difference in interaction energies, we examined the interacting structure of Leu133/Ile188 with N1, N4 and N5. As shown in Fig. 8(a), the closest distance between N1 and the CH_3 group of Leu133 is 2.4 Å, while the other parts of the Leu133 side chain is far away from N1. As a result, the interaction between Leu133 and N1 is weak. In the same way, as shown in Fig. 8(c), N5 and Leu133 are not directly interacting with each other. On the other hand, the CH_2–CH_3 group of N4 is located close to the CH_3 group of Leu133, as shown in Fig. 8(b), so that the hydrogen atoms of both the groups have repulsive interactions. It is thus elucidated from Fig. 8 that the configuration of one hexagonal ring of N4 and its CH_2–CH_3 group cause the repulsive interaction between N4 and Leu133.

Fig. 9 compares the interacting structures between Ile188 and N1, N4 and N5. As shown in Fig. 9(a), the two oxygen atoms of N1 are close (3.7 and 4.1 Å) to the oxygen atom of Ile188 backbone, resulting in the repulsions between N1 and Ile188. On the other hand, in the TLN–N4 (Fig. 9b) and TLN–N5 (Fig. 9c) complexes, there is no strong repulsive interaction between Ile188 and N4/N5, although the CH_3 group of Ile188 is close to these inhibitors. As shown in Figs. 8 and 9, the difference in the terminating groups of one of the hexagonal rings of N1, N4 and N5 inhibitors affects the configurations of the other hexagonal rings, resulting in their different interactions with Leu133 and Ile188. The present results elucidate that N5 dose not have repulsive forces with Leu133 and Ile188, because N5 has a planar structure and the terminating groups of the two hexagonal rings are not close to Lue133 and Ile188. It is thus expected that inhibitors with a 6-membered ring, which not interact repulsively to Leu133 and Leu188 of TLN, can bind in the ligand binding pocket of TLN.

The N2 inhibitor has the largest binding affinity to TLN in the previous experimental study [29] as well as in the present calculation (Table 1). As shown in Fig. 1, N2 is larger than the other inhibitors and has a dodecyl chain ($-(CH_2)_{11}-CH_3$) as well as pentagonal and hexagonal rings. It is expected that the dodecyl chain may contribute to the strong binding affinity between N2 and TLN. We then segmented N2 into two fragments: the ring and the chain. By means of the MFMO method, we investigated the interaction energies between these fragments and TLN to elucidate the effect of the dodecyl chain on the binding between N2 and TLN. Fig. 10 shows the interaction energies between each fragment and each amino acid residue of TLN or solvating water molecules. The ring

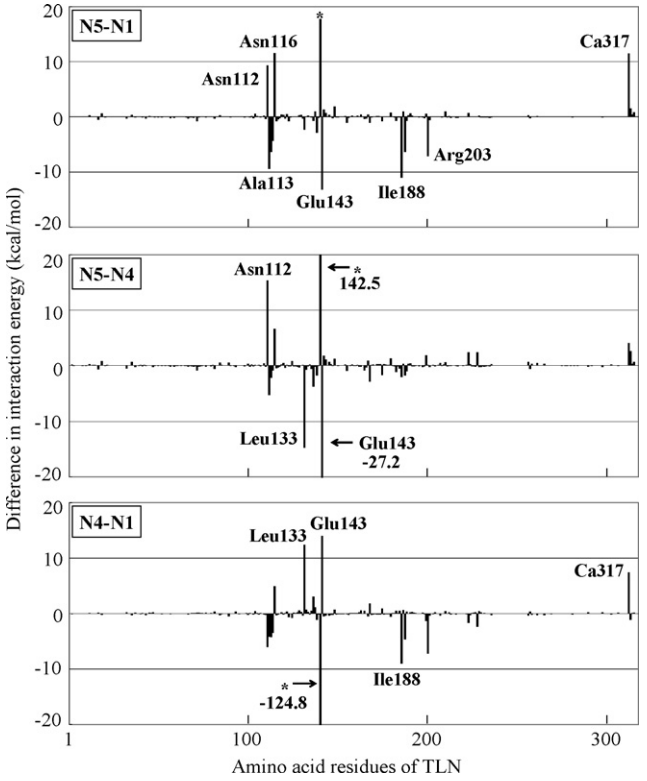

Fig. 7. Differences in interaction energies among the TLN–N1, TLN–N4 and TLN–N5 complexes. The asterisk indicates the fragment composed of Zn ion, His142, His146 and Glu166 residues of TLN existing near the Zn ion.

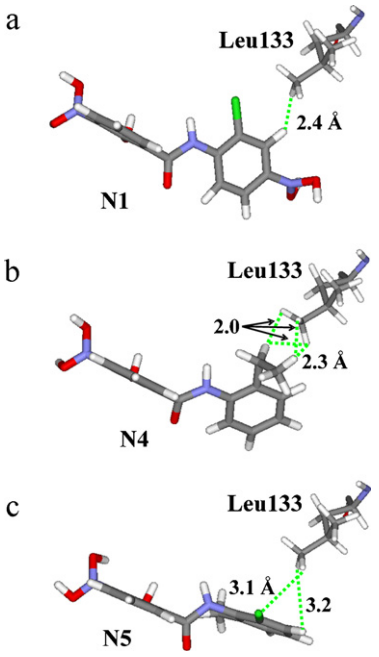

Fig. 8. Interacting structures between Leu133 of TLN and (a) N1, (b) N4 and (c) N5. Chlorine, hydrogen, carbon, oxygen and nitrogen atoms are shown in green, white, gray, red and blue colors, respectively. (For interpretation of the references to color in this figure legend, the reader is referred to the web version of the article.)

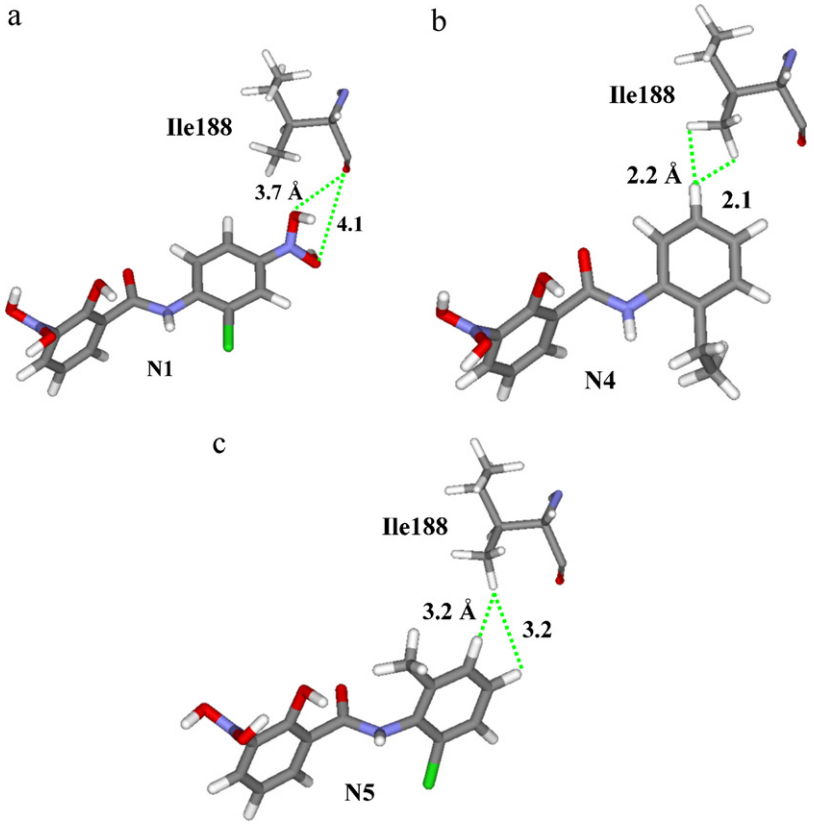

Fig. 9. Interacting structures between Ile188 of TLN and (a) N1, (b) N4 and (c) N5. Chlorine, hydrogen, carbon, oxygen and nitrogen atoms are shown in green, white, gray, red and blue colors, respectively. (For interpretation of the references to color in this figure legend, the reader is referred to the web version of the article.)

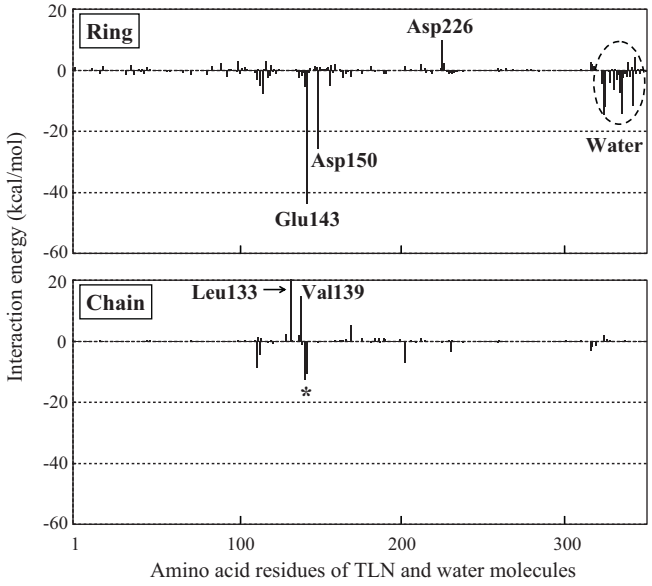

Fig. 10. Interaction energies between amino acid residues of TLN or water molecules and two fragments of N2. The asterisk indicates the fragment composed of Zn ion, His142, His146 and Glu166 residues of TLN existing near the Zn ion.

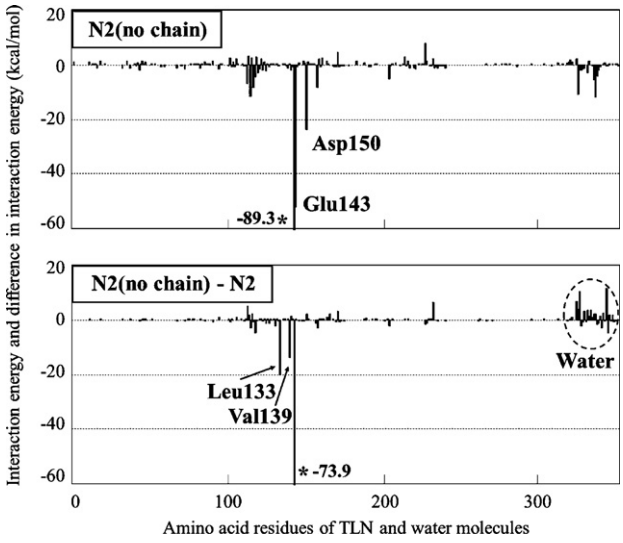

Fig. 12. Interaction energies between amino acid residues of TLN or water molecules and the N2(no chain), and the difference in the interaction energies between the TLN–N2(no chain) and TLN–N2 complexes. The asterisk indicates the fragment composed of Zn ion, His142, His146 and Glu166 residues of TLN existing near the Zn ion.

fragment interacts strongly with Glu143, Asp150 and Asp226 as well as water molecules. On the other hand, the chain fragment interacts repulsively with Leu133 and Val139. The total interaction energies between all amino acid residues of TLN and the ring and the chain fragments are evaluated to be −170 and −2.2 kcal/mol, respectively. Therefore, it is elucidated that the direct contribution of the chain group of N2 to the TLN–N2 binding is small. We would suppose that the chain group plays a role for stabilizing the ring group of N2 near to the Glu143 and Asp150 of TLN and for aggregating water molecules around the ring group of N2.

3.3. Proposal of a novel potent inhibitor to TLN

As indicated in Fig. 10, the chain group of N2 was found to have a small contribution to the binding between TLN and N2. We thus constructed a novel ligand without the chain group of N2 and investigated its specific interactions to TLN by using the *ab initio* molecular simulations. Fig. 11 shows the structures of N2 and the novel ligand, which is defined as N2(no chain) below. In the solvated TLN–N2(no chain) complex, only the structure of N2(no chain) and the positions of hydrogen atoms and solvating water molecules were optimized by AMBER9 [35], and the electronic states of the optimized structure were investigated by the MFMO method.

As listed in the last line of Table 1, the estimated binding energy between TLN and N2(no chain) is −135.4 kcal/mol, which is larger than that for the TLN–N2 complex, indicating that the novel N2(no

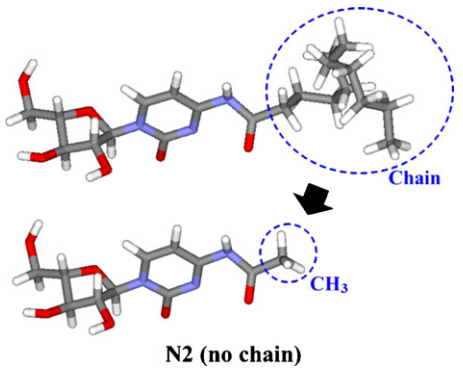

Fig. 11. Structures of N2 ligand and our proposed ligand N2(no chain) without the chain part of N2. Hydrogen, carbon, oxygen and nitrogen atoms are shown in white, gray, red and blue colors, respectively.

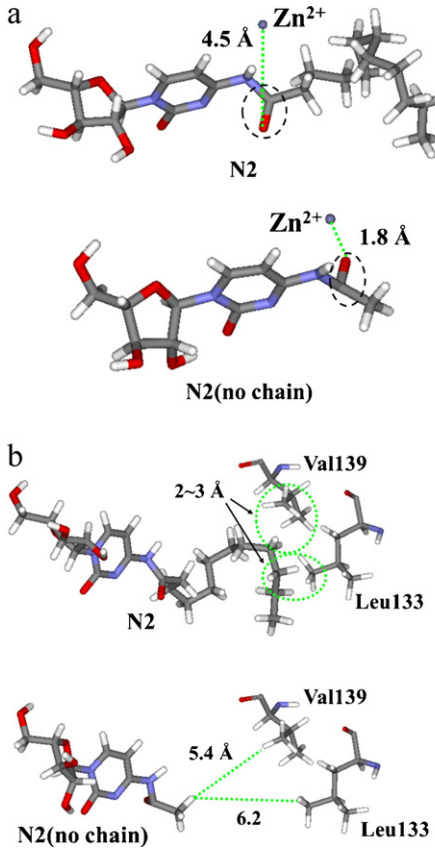

Fig. 13. Interacting structures between N2/N2(no chain) and (a) Zn ion and (b) Leu133 and Val139 of TLN. Hydrogen, carbon, oxygen and nitrogen atoms are shown in white, gray, red and blue colors, respectively. (For interpretation of the references to color in this figure legend, the reader is referred to the web version of the article.)

chain) ligand can bind to TLN more strongly than N2. To elucidate the origin of this result, the interaction energies between N2(no chain) and each TLN residue or water molecules were investigated and compared with those of TLN–N2. As indicated in Fig. 12, N2(no chain) has large attractive interactions with the Zn group and Glu143 of TLN, while the repulsive interactions between N2 and Leu133/Val139 of TLN shown in Fig. 10 disappear in the TLN–N2(no chain) complex. These changes in the interactions are likely to cause the large binding energy between TLN and N2(no chain).

To elucidate the reason for that N2(no chain) interacts strongly with the Zn group of TLN, we furthermore investigated the structure around the Zn group for both the TLN–N2 and TLN–N2(no chain) complexes. As shown in Fig. 13(a), the oxygen atom of the C=O group of N2 is 4.5 Å away from the Zn ion in the TLN–N2 complex. On the other hand, in the TLN–N2(no chain) complex, the C=O group can change its conformation to interact with the Zn ion, because of the removal of the chain part. As a result, the distance between the Zn ion and the oxygen atom becomes 1.8 Å, leading to the large attractive interaction. In addition, the repulsive interactions between the chain part of N2 and the Val139/Leu133 residues of TLN shown in Fig. 13(b) are diminished by removing the chain part. In consequence, our calculations indicate that the proposed N2(no chain) ligand binds more strongly to TLN than N2 and has possibilities as potent TLN inhibitor.

4. Conclusions

In the present study, we optimized the solvated structures of the complexes of TLN with the inhibitors Nx, which were identified as TLN inhibitors in our previous experimental and molecular modeling study [29]. In addition, the specific interactions between each amino acid residue of TLN and Nx were investigated by the *ab initio* MFMO method at an electronic level to indicate the following points:

1. The computed binding energies between TLN and Nx are qualitatively comparable to the experimentally obtained binding affinity [29] between TLN and Nx.
2. N2 binds most strongly to TLN. The Zn group, Asp150 and Leu133 and solvating water molecules contribute strongly to the binding between TLN and N2.
3. The ring group of N2 gives the main contribution to the binding between TLN and N2, while the chain part of N2 has almost no contribution.
4. The proposed virtual ligand without the chain part of N2 is predicted to bind stronger to TLN than N2, indicating that this ligand may be a potent TLN inhibitor.
5. N1, N4 and N5 interact with TLN differently, in spite of that their chemical structures are quite similar to each other. N5 is stabilized in the ligand binding pocket of TLN, because it has a 6-membered ring, which not interact repulsively to Leu133 and Leu188 of TLN.

Acknowledgements

This work was supported by JSPS Grant-in-Aid for Challenging Exploratory Research (No. 22650061), MEXT Grant-in-Aid for JSPS Fellows (K.D., No. 20.8138), the grants from the Murata Science Foundation, the Iketani Science and Technology Foundation, the Tatematsu Foundation and the CASIO Science Promotion Foundation. This work was also supported by the Notur project (Norway) by access to supercomputing facilities at University of Tromsø, Norway.

References

[1] S.A. Latt, B. Holmquist, B.L. Vallee, Thermolysin: a zinc metalloenzyme, Biochem. Biophys. Res. Commun. 37 (1969) 333–339.
[2] K. Inouye, S.B. Lee, B. Tonomura, Effect of amino acid residues at the cleavable site of substrates on the remarkable activation of thermolysin by salts, Biochem. J. 315 (1996) 133–138.
[3] J. Feder, L.R. Garrett, B.S. Wildi, Studies on the role of calcium in thermolysin, Biochemistry 10 (1971) 4552–4556.
[4] P. Bartlett, C. Marlowe, Possible role for water dissociation in the slow binding of phosphorus-containing transition-state-analog inhibitors of thermolysin, Biochemistry 26 (1987) 8553–8561.
[5] A. de Kreij, B. van den Burg, O. Veltman, G. Vriend, G. Venema, V. Eijsink, The effect of changing the hydrophobic S1' subsite of thermolysin-like proteases on substrate specificity, Eur. J. Biochem. 268 (2001) 4985–4991.
[6] M. Bruins, A. Janssen, R. Boom, Thermozymes and their applications, Appl. Biochem. Biotechnol. 90 (2001) 155–186.
[7] G. Haki, S. Rakshit, Developments in industrially important thermostable enzymes: a review, Bioresour. Technol. 89 (2003) 17–34.
[8] B. Matthews, J. Jansonius, P. Colman, B. Schoenborn, D. Dupourque, Three-dimensional structure of thermolysin, Nature New Biol. 238 (1972) 37–41.
[9] K. Oyama, S. Nishimura, Y. Nonaka, K. Kihara, T. Hashimoto, Synthesis of an aspartame precursor by immobilized thermolysin in an organic solvent, J. Org. Chem. 46 (1981) 5241–5242.
[10] K. Inouye, M. Kusano, Y. Hashida, M. Minoda, K. Yasukawa, Engineering, expression, purification, and production of recombinant thermolysin, Biotechnol. Annu. Rev. 13 (2007) 43–64.
[11] N. Gresh, B. Roques, Thermolysin-inhibitor binding: effect of the His 231 Ala mutation on the relative affinities of thiolate versus phosphoramidate inhibitors-a model theoretical investigation incorporating a continuum reaction field hydration model, Peptide Sci. 41 (1997) 145–164.
[12] D. Hangauer, A. Monzingo, B. Matthews, An interactive computer graphics study of thermolysin-catalyzed peptide cleavage and inhibition by N-carboxymethyl dipeptides, Biochemistry 23 (1984) 5730–5741.
[13] C. Kam, N. Nishino, J. Powers, Inhibition of thermolysin and carboxypeptidase A by phosphoramidates, Biochemistry 18 (1979) 3032–3038.
[14] T. Komiyama, H. Suda, T. Aoyagi, T. Takeuchi, H. Umezawa, K. Fujimoto, S. Umezawa, Studies on inhibitory effect of phosphoramidon and its analogs on thermolysin, Arch. Biochem. Biophys. 171 (1975) 727–731.
[15] S. Seeram, K. Hiraga, A. Saji, M. Tashiro, K. Oda, Identification of reactive site of a proteinaceous metalloproteinase inhibitor from *Streptomyces nigrescens* TK-23, J. Biochem. 121 (1997) 1088–1095.
[16] D. Tronrud, A. Monzingo, B. Matthews, Crystallographic structural analysis of phosphoramidates as inhibitors and transition-state analogs of thermolysin, Eur. J. Biochem. 157 (1986) 261–268.
[17] S. Antonczak, G. Monard, M. Ruiz-Lpez, J. Rivail, Insights in the peptide hydrolysis mechanism by thermolysin: a theoretical QM/MM study, J. Mol. Model. 6 (2000) 527–538.
[18] D. Holland, A. Hausrath, D. Juers, B. Matthews, Structural analysis of zinc substitutions in the active site of thermolysin, Protein Sci. 4 (1995) 1955–1965.
[19] W. Mock, M. Aksamawati, Binding to thermolysin of phenolate-containing inhibitors necessitates a revised mechanism of catalysis, Biochem. J. 302 (1994) 57–68.
[20] W. Mock, D. Stanford, Arazoformyl dipeptide substrates for thermolysin: confirmation of a reverse protonation catalytic mechanism, Biochemistry 35 (1996) 7369–7377.
[21] V. Pelmenschikov, M. Blomberg, P. Siegbahn, A theoretical study of the mechanism for peptide hydrolysis by thermolysin, J. Biol. Inorg. Chem. 7 (2002) 284–298.
[22] S. Toma, S. Campagnoli, E. Gregoriis, R. Gianna, I. Margarit, M. Zamai, G. Grandi, Effect of Glu-143 and His-231 substitutions on the catalytic activity and secretion of *Bacillus subtilis* neutral protease, Protein Eng. 2 (1989) 359–364.
[23] B. Altincicek, M. Linder, D. Linder, K.T. Preissner, A. Vilcinskas, Microbial metalloproteinases mediate sensing of invading pathogens and active innate immune responses in the lepidopteran model host galleria mellonella, Infect. Immun. 75 (2007) 175–183.
[24] C. Supuran, A. Scozzafava, A. Mastrolorenzo, Bacterial proteases: current therapeutic use and future prospects for the development of new antibiotics, Expert Opin. Ther. Pat. 11 (2001) 221–259.
[25] J. Travis, J. Potempa, Bacterial proteinases as targets for the development of second-generation antibiotics, Biochim. Biophys. Acta 1477 (2000) 35–50.
[26] I. Gomez-Monterrey, A. Beaumont, P. Nemecek, B.P. Roques, M.C. Fournie-Zaluski, New thiol inhibitors of neutral endopeptidase EC 3.4.24.11: synthesis and enzyme active-site recognition, J. Med. Chem. 37 (1994) 1865–1873.
[27] R. Bohacek, C. McMartin, W. Guida, The art and practice of structure-based drug design: a molecular modeling perspective, Med. Res. Rev. 16 (1996) 3–50.
[28] G. Tiraboschi, N. Jullian, V. Thery, S. Antonczak, M. Fournie-Zaluski, B. Roques, A three-dimensional construction of the active site (region 507–749) of human neutral endopeptidase (EC. 3.4. 24.11), Protein Eng. 12 (1999) 141–149.
[29] M.T.H. Khan, O.M. Fuskevag, I. Sylte, Discovery of potent thermolysin inhibitors using structure based virtual screening and binding assays, J. Med. Chem. 52 (2009) 48–61.

[30] R. Abagyan, M. Totrov, Biased probability Monte Carlo conformational searches and electrostatic calculations for peptides and proteins, J. Mol. Biol. 235 (1994) 983–1002.
[31] R. Abagyan, M. Totrov, D. Kuznetsov, ICM-a new method for protein modeling and design: applications to docking and structure prediction from the distorted native conformation, J. Comput. Chem. 15 (1994) 488–506.
[32] M. Totrov, R. Abagyan, Efficient parallelization of the energy, surface, and derivative calculations for internal coordinate mechanics, J. Comput. Chem. 15 (1994) 1105–1112.
[33] M.T.H. Khan, W. Yimingjiang, I. Sylte, Binding modes, pharmacophore modelling, and predictions of absorption, distribution and toxicity of thermolysin inhibitors, Mini-Rev. Med. Chem. (2011).
[34] M.T.H. Khan, R. Khan, W. Yimingjiang, M. Arfan, M. Ahmed, I. Sylte, Identification of novel quinazolin-4 (3H)-ones as inhibitors of thermolysin, the prototype of the M4 family of proteinases, Bioorg. Med. Chem. 18 (2010) 4317–4327.
[35] D. Case, T. Darden, T. Cheatham III, C. Simmerling, J. Wang, R. Duke, R. Luo, K. Merz, D. Pearlman, M. Crowley, AMBER 9, University of California, San Francisco, 2006.
[36] W. Cornell, P. Cieplak, C. Bayly, I. Gould, K. Merz, D. Ferguson, D. Spellmeyer, T. Fox, J. Caldwell, P. Kollman, A second generation force field for the simulation of proteins, nucleic acids, and organic molecules, J. Am. Chem. Soc. 117 (1995) 5179–5197.
[37] W. Jorgensen, J. Chandrasekhar, J. Madura, R. Impey, M. Klein, Comparison of simple potential functions for simulating liquid water, J. Chem. Phys. 79 (1983) 926–935.
[38] B. Besler, K. Merz, P. Kollman, Atomic charges derived from semiemprical methods, J. Comput. Chem. 11 (1990) 431–439.
[39] C. Lee, W. Yang, R. Parr, Development of the Colle–Salvetti correlation-energy formula into a functional of the electron density, Phys. Rev. B 37 (1988) 785–789.
[40] M.J. Frisch, G.W. Trucks, H.B. Schlegel, G.E. Scuseria, M.A. Robb, J.R. Cheeseman, J.A. Montgomery Jr., T. Vreven, K.N. Kudin, J.C. Burant, J.M. Millam, S.S. Iyengar, J. Tomasi, V. Barone, B. Mennucci, M. Cossi, G. Scalmani, N. Rega, G.A. Petersson, H. Nakatsuji, M. Hada, M. Ehara, K. Toyota, R. Fukuda, J. Hasegawa, M. Ishida, T. Nakajima, Y. Honda, O. Kitao, H. Nakai, M. Klene, X. Li, J.E. Knox, H.P. Hratchian, J.B. Cross, V. Bakken, C. Adamo, J. Jaramillo, R. Gomperts, R.E. Stratmann, O. Yazyev, A.J. Austin, R. Cammi, C. Pomelli, J.W. Ochterski, P.Y. Ayala, K. Morokuma, G.A. Voth, P. Salvador, J.J. Dannenberg, V.G. Zakrzewski, S. Dapprich, A.D. Daniels, M.C. Strain, O. Farkas, D.K. Malick, A.D. Rabuck, K. Raghavachari, J.B. Foresman, J.V. Ortiz, Q. Cui, A.G. Baboul, S. Clifford, J. Cioslowski, B.B. Stefanov, G. Liu, A. Liashenko, P. Piskorz, I. Komaromi, R.L. Martin, D.J. Fox, T. Keith, M.A. Al-Laham, C.Y. Peng, A. Nanayakkara, M. Challacombe, P.M.W. Gill, B. Johnson, W. Chen, M.W. Wong, C. Gonzalez, J.A. Pople, Gaussian 03, Revision E. 01, Gaussian, Inc., Wallingford, CT, 2004.
[41] D. Fedorov, T. Ishida, K. Kitaura, Multilayer formulation of the fragment molecular orbital method (FMO), J. Phys. Chem. A 109 (2005) 2638–2646.
[42] K. Kitaura, E. Ikeo, T. Asada, T. Nakano, M. Uebayasi, Fragment molecular orbital method: an approximate computational method for large molecules, Chem. Phys. Lett. 313 (1999) 701–706.
[43] K. Kitaura, T. Sawai, T. Asada, T. Nakano, M. Uebayasi, Pair interaction molecular orbital method: an approximate computational method for molecular interactions, Chem. Phys. Lett. 312 (1999) 319–324.
[44] T. Nakano, T. Kaminuma, T. Sato, Y. Akiyama, M. Uebayasi, K. Kitaura, Fragment molecular orbital method: application to polypeptides, Chem. Phys. Lett. 318 (2000) 614–618.
[45] T. Nakano, T. Kaminuma, T. Sato, K. Fukuzawa, Y. Akiyama, M. Uebayasi, K. Kitaura, Fragment molecular orbital method: use of approximate electrostatic potential, Chem. Phys. Lett. 351 (2002) 475–480.
[46] A. Tagami, N. Ishibashi, D. Kato, N. Taguchi, Y. Mochizuki, H. Watanabe, M. Ito, S. Tanaka, *Ab initio* quantum-chemical study on emission spectra of bioluminescent luciferases by fragment molecular orbital method, Chem. Phys. Lett. 472 (2009) 118–123.
[47] M. Ito, K. Fukuzawa, T. Ishikawa, Y. Mochizuki, T. Nakano, S. Tanaka, *Ab initio* fragment molecular orbital study of molecular interactions in liganded retinoid X receptor: specification of residues associated with ligand inducible information transmission, J. Phys. Chem. B 112 (2008) 12081–12094.
[48] K. Fukuzawa, Y. Mochizuki, S. Tanaka, K. Kitaura, T. Nakano, Molecular interactions between estrogen receptor and its ligand studied by the *ab initio* fragment molecular orbital method, J. Phys. Chem. B 110 (2006) 16102–16110.
[49] K. Fukuzawa, Y. Komeiji, Y. Mochizuki, T. Nakano, S. Tanaka, Intra- and intermolecular interactions between cyclic-AMP receptor protein and DNA: *ab initio* fragment molecular orbital study, J. Comput. Chem. 27 (2006) 948–960.
[50] I. Kurisaki, K. Fukuzawa, Y. Komeiji, Y. Mochizuki, T. Nakano, J. Imada, A. Chmielewski, S.M. Rothstein, H. Watanabe, S. Tanaka, Visualization analysis of inter-fragment interaction energies of CRP–cAMP–DNA complex based on the fragment molecular orbital method, Biophys. Chem. 130 (2007) 1–9.
[51] K. Dedachi, M.T.H. Khan, I. Sylte, N. Kurita, A combined simulation with *ab initio* MO and classical vibrational analysis on the specific interactions between thermolysin and dipeptide ligands, Chem. Phys. Lett. 479 (2009) 290–295.
[52] K. Dedachi, T. Hirakawa, S. Fujita, M.T.H. Khan, I. Sylte, N. Kurita, Specific interactions and binding free energies between thermolysin and dipeptides: molecular simulations combined with *ab initio* molecular orbital and classical vibrational analysis, J. Comput. Chem. (2011), doi:10.1002/jcc.21887.
[53] G.M. Morris, D.S. Goodsell, R.S. Halliday, R. Huey, W.E. Hart, R.K. Belew, A.J. Olson, Automated docking using a lamarckian genetic algorithm and an empirical binding free energy function, J. Comput. Chem. 19 (1998) 1639–1662.